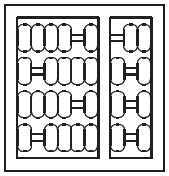

INSTITUTO DE COMPUTAÇÃO
UNIVERSIDADE ESTADUAL DE CAMPINAS

Approximation Error Maps

Anamaria Gomide *Jorge Stolfi*

Technical Report - IC-01-001 - Relatório Técnico

February - 2001 - Fevereiro

Approximation Error Maps

Anamaria Gomide and Jorge Stolfi
Inst. de Computação, Univ. Estadual de Campinas
Caixa Postal 6176, 13081-970 Campinas, SP.
{anamaria,stolfi}@ic.unicamp.br

Abstract

Let $\mathcal{F}$ and $\mathcal{A}$ be two linear function spaces defined on some domain Ω. Let $\|\cdot\|$ be a vector semi-norm for the space $\mathcal{A} + \mathcal{F}$. We consider here the question of how well $\mathcal{A}$ approximates $\mathcal{F}$ in the sense of the metric $\|\cdot\|$. Global error measures are insufficiently informative when the space $\mathcal{A}$ is not spatially homogeneous. We introduce here the concept of *approximation error map*, a mathematical description of how the approximation errors are distributed over the domain — not for a single function $f \in \mathcal{F}$, but for all such functions at once. We illustrate this concept by computing the error maps of several harmonic spline spaces on the circle and on the sphere.

1 Introduction

Let $\mathcal{F}$ and $\mathcal{A}$ be two finite-dimensional vector spaces, not necessarily disjoint, of functions defined on some domain Ω with values in $\mathbf{R}$. Let $\|\cdot\|$ be a vector semi-norm for the space $\mathcal{A} + \mathcal{F}$. For any function $f \in \mathcal{F}$, we define its *best approximation* as the function $f^{\mathcal{A}} \in \mathcal{A}$ that minimizes the error $\left\|f - f^{\mathcal{A}}\right\|$. Our goal in this report is to understand how well $\mathcal{A}$ approximates a general function from $\mathcal{F}$, in the sense of the metric $\|\cdot\|$; and, specifically, how the error is distributed over the domain Ω.

We will refer to $\mathcal{A}$ and $\mathcal{F}$ as the *approximation* and *gauge spaces*, respectively. We will assume that the semi-norm $\|\cdot\|$ is such that the best approximation exists and is unique. For this, it suffices that the $\|\cdot\|$-balls *in the subspace* $\mathcal{A}$ be strictly convex.

Observe that $(\alpha f)^{\mathcal{A}} = \alpha(f^{\mathcal{A}})$ and $\|\alpha f\| = |\alpha| \, \|f\|$ for any real constant α. Therefore, we can confine the analysis of approximation errors to the *unit $\mathcal{F}$-sphere* $\mathcal{F}_1 = \{ f \in \mathcal{F} : \|f\| = 1 \}$.

1.1 Global error measures

Usually, the effectiveness of the approximation space $\mathcal{A}$ is measured by a single number $\left\|f - f^{\mathcal{A}}\right\|$—either for the worst-case function $f \in \mathcal{F}_1$, or averaged over all functions $f \in \mathcal{F}_1$. The general root-mean-power average is

$$\sigma^*_{p,\mathcal{A},\mathcal{F}} = \left[\int_{\mathcal{F}_1} \left\|f - f^{\mathcal{A}}\right\|^p \, df\right]^{1/p} \Bigg/ \left[\int_{\mathcal{F}_1} 1 \, df\right]^{1/p} \tag{1}$$

Observe that integrals are taken over the function space $\mathcal{F}_1$, not over the domain Ω. The worst-case error is the limit

$$\begin{aligned} \mu^*_{\mathcal{A},\mathcal{F}} &= \lim_{p \to +\infty} \sigma^*_{p,\mathcal{A},\mathcal{F}} \\ &= \sup \left\{ \left\| f - f^{\mathcal{A}} \right\| \,:\, f \in \mathcal{F}_1 \right\} \end{aligned} \tag{2}$$

1.2 Uniform approximation spaces

A global error measure such as $\mu^*_{\mathcal{A},\mathcal{F}}$ or $\sigma^*_{p,\mathcal{A},\mathcal{F}}$ is generally sufficient when all points of Ω are equivalent with respect to the quality of approximation. More formally, we say that a normed function space $\mathcal{X}$ is *uniform* over Ω if there is some family Φ of maps from Ω to Ω that preserves $\mathcal{X}$ and its norm $\|\cdot\|$, and which can take any point of Ω to any other point. Obviously, if both $\mathcal{A}$ and $\mathcal{F}$ are uniform under the same family Φ, then $\mathcal{A}$ approximates $\mathcal{F}$ equally well at all points of Ω. (Of course, for any *specifc* function $f \in \mathcal{F}$, the error $f - f^{\mathcal{A}}$ will usually vary over Ω.)

A natural example of uniform function space is $\mathcal{Y}^d_n$, the set of all harmonic functions on the sphere $\mathbf{S}^d$ of a given maximum order n, with any L_p norm; this space is preserved by the family of rigid rotations of $\mathbf{S}^d$.

2 Evaluation of non-uniform approximation spaces

There are however many important approximation spaces $\mathcal{A}$ which are not uniform. A familiar example is the space of polynomials or trigonometric series defined on a bounded region $\Omega \subseteq \mathbf{R}^n$. Another example is the space of the piecewise polynomial splines of fixed order and continuity defined over a fixed decomposition of the domain. Wavelet spaces truncated to a fixed order povide yet another example. When analyzing the effectiveness of such spaces, it makes sense to ask how the approximation error is expected to vary over the domain Ω.

Indeed, the very notion of adaptive splines is based on the premise that, by using a domain decomposition that is finer in a particular region of Ω, we can improve the accuracy of the approximation in that region, but avoid the cost of using a finer decomposition over the whole domain.

2.1 Approximation error map

In order to display the spatial distribution of the errors, we define the *root mean power approximation error map of $\mathcal{F}$ by $\mathcal{A}$* as the function $\mu_{\mathcal{A},\mathcal{F}}$ of Ω to $\mathbf{R}$ defined by

$$\sigma_{p,\mathcal{A},\mathcal{F}}(x) = \left[\int_{\mathcal{F}_1} \left| f(x) - f^{\mathcal{A}}(x) \right|^p \, df \right]^{1/p} \Big/ \left[\int_{\mathcal{F}_1} 1 \, df \right]^{1/p} \tag{3}$$

Note that the integrals are taken over the function space $\mathcal{F}_1$, not over the domain Ω. Note also that $\sigma_{p,\mathcal{A},\mathcal{F}}(x)$ is not the error for a *specific* function f, but rather the *average* error *at the point* x for a *generic* function f in $\mathcal{F}_1$.

As a limiting case, we define also the *worst-case approximation error map of* $\mathcal{F}$ *by* $\mathcal{A}$ as the function

$$\begin{aligned} \mu_{\mathcal{A},\mathcal{F}}(x) &= \lim_{p \to +\infty} \sigma_{p,\mathcal{A},\mathcal{F}}(x) \\ &= \sup \{ \, |f(x) - f^{\mathcal{A}}(x)| \, : \, f \in \mathcal{F}_1 \, \} \end{aligned} \tag{4}$$

Again note that the supremum is taken over $\mathcal{F}_1$, not over Ω; and that $\mu_{\mathcal{A},\mathcal{F}}(x)$ is not the error at x for a *single* function f, but rather the error for the function f in $\mathcal{F}_1$ that is worst *for that particular* x.

A plot of $\sigma_{p,\mathcal{A},\mathcal{F}}(x)$ or $\mu_{\mathcal{A},\mathcal{F}}(x)$ over Ω should show at a glance how well $\mathcal{A}$ approximates $\mathcal{F}$ in different parts of the domain, for all functions of $\mathcal{F}$ at once.

3 Computing the approximation error map

Formulas **??** become more tractable when the function metric $\|\cdot\|$ is the "Euclidean" L_2 norm $\|f\| = [\int_\Omega |f(x)|^2 \, dx]^{1/2}$ defined on the space $\mathcal{A} + \mathcal{F}$ — in other words, when $\|f\|^2 = \langle f, f \rangle$ where $\langle f, g \rangle = \int_\Omega f(x) g(x) \, dx$. We make this assumption in the remainder of this section.

In that case, it is well-known that $f^{\mathcal{A}}$ is a linear function of f, namely the orthogonal projection of f onto the subspace $\mathcal{A}$. Moreover, $\mu_{\mathcal{A},\mathcal{F}}$ is simply $|\sin\theta|$ where θ is the angle between the two subspaces.

3.1 Explicit formula for σ

Let's suppose $\mathcal{A}$ and $\mathcal{F}$ are disjoint, and let $\phi_1, .. \phi_n$ be an orthonormal basis for $\mathcal{F}$. Let $\alpha_i = \phi_i^{\mathcal{A}}$ for all i, and let $\varepsilon_i = \phi_i - \alpha_i$. We will call ϕ, α, and ε the *gauge*, *approximation*, and *error bases*, respectively (even though α_i and ε_i need not be independent).

The average error map $\sigma_{p,\mathcal{A},\mathcal{F}}(x)$ can be developed into an explicit formula in terms of the error basis:

$$\begin{aligned} \sigma_{p,\mathcal{A},\mathcal{F}}(x) &= \left[\int_{\mathbf{S}^{n-1}} \left| (\sum_i c_i \phi_i)(x) - (\sum_i c_i \phi_i)^{\mathcal{A}}(x) \right|^p dc \right]^{1/p} \Bigg/ \left[\int_{\mathbf{S}^{n-1}} 1 \, dc \right]^{1/p} \\ &= \left[\frac{1}{A_n} \int_{\mathbf{S}^{n-1}} \left| \sum_i c_i (\phi_i - \alpha_i)(x) \right|^p dc \right]^{1/p} \\ &= \left[\frac{1}{A_n} \int_{\mathbf{S}^{n-1}} \left| \sum_i c_i \varepsilon_i(x) \right|^p dc \right]^{1/p} \end{aligned} \tag{5}$$

where A_n is the measure of $\mathbf{S}^{n-1}$,

$$A_n = \frac{2\pi^{\frac{n}{2}}}{\Gamma(\frac{n}{2})} \tag{6}$$

Note that $\sum_i c_i \varepsilon_i(x)$ is the dot product of the vectors $c = (c_1, c_2, \ldots, c_n)$ and $\varepsilon(x) = (\varepsilon_1(x), \varepsilon_2(x), \ldots \varepsilon_n(x))$; it depends only on the angle θ between those two vectors, and

is constant over the slice of $\mathbf{S}^{n-1}$ where θ is constant. The measure of that slice is $A_{n-1}\,|\sin\theta|^{n-1}\,d\theta$. Therefore,

$$\begin{aligned}
\sigma_{p,\mathcal{A},\mathcal{F}}(x) &= \left[\frac{1}{A_n}\int_0^\pi |c|\,|\varepsilon(x)|\,|\cos\theta|^p\,A_{n-1}\,|\sin\theta|^{n-1}\,d\theta\right]^{1/p} \\
&= |\varepsilon(x)|\left[\frac{A_{n-1}}{A_n}\int_0^\pi |\cos\theta|^p\,|\sin\theta|^{n-1}\,d\theta\right]^{1/p} \\
&= |\varepsilon(x)|\left[\frac{(\Gamma(\frac{n}{2}))^2\Gamma(\frac{p+1}{2})}{\sqrt{\pi}\Gamma(\frac{n-1}{2})\Gamma(\frac{p+1+n}{2})}\right]^{1/p} \qquad (7)
\end{aligned}$$

3.2 Explicit formula for μ

The worst-case error map $\mu_{\mathcal{A},\mathcal{F}}$ can be obtained by taking p to the limit $+\infty$ in formula (**??**), or directly, as follows. From formula (4),

$$\begin{aligned}
\mu_{\mathcal{A},\mathcal{F}}(x) &= \sup\{\left|(\sum_i c_i\phi_i)(x) - (\sum_i c_i\phi_i)^{\mathcal{A}}(x)\right| \,:\, \left\|\sum_i c_i\phi_i\right\| = 1\} \\
&= \sup\{\left|\sum_i c_i(\phi_i - \alpha_i)(x)\right| \,:\, c \in \mathbf{S}^{n-1}\} \\
&= \sup\{\left|\sum_i c_i\varepsilon_i(x)\right| \,:\, c \in \mathbf{S}^{n-1}\} \qquad (8)
\end{aligned}$$

By considering the effect of negating each c_i, it is easy to see that the absolute value in the last formula is superfluous, i.e.

$$\mu_{\mathcal{A},\mathcal{F}}(x) = \sup\left\{\sum_i c_i\varepsilon_i(x) \,:\, c \in \mathbf{S}^{n-1}\right\} \qquad (9)$$

Formula (9) is the supremum of a linear functional with coefficients $\varepsilon_i(x)$ over the sphere $\mathbf{S}^{n-1}$; which is achieved at the point $c^*(x)$ of $\mathbf{S}^{n-1}$ that is collinear with the coefficient vector, namely

$$c_i^*(x) = \frac{\varepsilon_i(x)}{\sqrt{\sum_j \varepsilon_j(x)^2}} \qquad (10)$$

whence

$$\mu_{\mathcal{A},\mathcal{F}}(x) = \sum_i c_i^*(x)\varepsilon_i(x) = \sqrt{\sum_j \varepsilon_j(x)^2} = |\varepsilon(x)| \qquad (11)$$

In summary, the error maps $\sigma_{p,\mathcal{A},\mathcal{F}}(x)$ and $\mu_{\mathcal{A},\mathcal{F}}(x)$ (which differ only by a constant factor) can be obtained by computing the approximation errors $\varepsilon_i(x)$ for each basis function $\phi_i(x)$, and combining them with the Euclidean norm $|\varepsilon(x)| = \sqrt{\sum_i(\varepsilon_i(x))^2}$.

4 Practical considerations

4.1 Connection between the function and point norms

The maps (4) and (3) will be more useful when there is a direct connection between the function-space norm $\|\cdot\|$ and the absolute value $|\cdot|$,used to compare functions values at a given point x, as in formulas 3–4 — namely, when

$$\|f\| = [\int_\Omega |f(x)|^q \, dx]^{1/q} \tag{12}$$

More generally, the functions values at x could be compared with a more complex norm $:\|\cdot\|:$, which could depend on x, take or derivatives of the function into account, etc. We will not pursue such extensions in this paper.

The connection (12) is not strictly necessary — at least when $\mathcal{A}$ and $\mathcal{F}$ are finite dimensional. However, it may not make much sense to choose the approximant $f^\mathcal{A}$ so as to minimize the function norm $\|\cdot\|$, and then analyze its accuracy using the absolute value norm $|\cdot|$, if there is no connection between the two.

Considering that the error map is relatively easy to compute when $\|\cdot\|$ is the L_2 norm (see section 3), and probably intractable otherwise, the connection expressed by formula 12 will probably hold in practice (with $q = 2$).

4.2 Choice of the gauge space

The approximation error map depends not only on the space $\mathcal{A}$, but also on the gauge space $\mathcal{F}$ and the error metric $\|f\|$. Therefore, the choice of $\mathcal{F}$ and $\|\cdot\|$ must be guided by the intended application.

For example, suppose the domain Ω is the circle or the sphere $\mathbf{S}^d$, and the application does not specify a preferred direction. Then we should choose $\mathcal{F}$ and $\|\cdot\|$ so that they are invariant under rotations of Ω — otherwise, any inhomogeneity in them may produce irrelevant artifacts in the error map. Also, if the functions to be approximated are expected to be smooth, and/or only their low frequencies are important, then the function in $\mathcal{F}$ should be smooth too. A natural choice for $\mathcal{F}$, in this case, are the circular or spherical harmonics up to a certain maximum order; and the metric $\|\cdot\|$can be simply the L_q norm over the sphere $\mathbf{S}^d$.

4.3 Essential dimensions

We will argue next that, for the L_2 function norm, the "interesting" part of the error map is determined by two "essential" subspaces $\mathcal{F}' \subseteq \mathcal{F}$ and $\mathcal{A}' \subseteq \mathcal{A}$, which are disjoint and such that $\dim \mathcal{F}' \geq \dim \mathcal{A}'$.

First, if the spaces $\mathcal{A}$ and $\mathcal{F}$ have a non-trivial intersection $\mathcal{V}$, and we split a function $f \in \mathcal{F}$ into its components $g \in \mathcal{V}$ and $h \perp \mathcal{V}$, we find that $f^\mathcal{A} = g + h^\mathcal{A}$; and that $h^\mathcal{A}$ is itself orthogonal to $\mathcal{V}$. Therefore, we can confine our attention to the complements $\mathcal{F}'$ and $\mathcal{A}'$ of $\mathcal{V}$ relative to $\mathcal{A}$ and $\mathcal{F}$, which are disjoint.

Let's then suppose that $\mathcal{A}$ and $\mathcal{F}$ are disjoint. If $\dim \mathcal{F} < \dim \mathcal{A}$, let $\mathcal{A}' \subset \mathcal{A}$ be projection of $\mathcal{F}$ onto $\mathcal{A}$, which contains all optimum approximants. Obviously, for any function f, we have $f^{\mathcal{A}} = f^{\mathcal{A}'}$, so we can confine our attention to the space $\mathcal{A}'$, which is still disjoint from $\mathcal{F}$ and satisfies $\dim \mathcal{F} \geq \dim \mathcal{A}'$.

5 Examples

5.1 Trigonometric splines on the circle

As an example, we now consider the approximation of function by trigonometric splines, of maximum frequency r, defined on a partition T of $\mathbf{S}^1$ into 4 equal arcs. This space coincides with the space $\mathcal{P}_{-1}^{r,2}[T]$ of non-homogeneous polynomial splines with no continuity constraints [4]. For the gauge space $\mathcal{F}$, we will use the family of trigonometric series truncated after a suitable maximum frequency $s \geq r$; which coincides with the space of general spherical polynomials (not splines) $\mathcal{P}^{s,2}$ for some $s \geq r$. Specifically, we take

- $\Omega =$ the unit circle $\mathbf{S}^1$;
- $\mathcal{A} = \mathcal{P}_{-1}^{r,2}[T]$ where T is the division of the circle into quadrants;
- $\mathcal{F} = \mathcal{P}^{s,2}$, for some $s \geq r$;
- $\|f\| = \sqrt{\langle f, f \rangle}$ where $\langle f, g \rangle = \int_{\mathbf{S}^1} f(\theta) g(\theta)\, dp$.

For the gauge space $\mathcal{F}_1$, we will use the *Fourier basis*, which can be written as

$$\phi_i(\theta) = \frac{1}{\sqrt{\pi}} \sin\left(i\theta + \frac{\pi}{4}\right) \tag{13}$$

where $i \in \{-s, ..., s\}$.

As observed in section 4, we can ignore the subspace $\mathcal{A}' = \mathcal{F} \cap \mathcal{A}$ of $\mathcal{A}$ generated by $\phi_{-r}, \ldots, \phi_r$. Moreover, we need to take s sufficienty large that $\dim \mathcal{F} \geq \dim \mathcal{A}$–, i.e. $(2s+1) \geq 4(2s+1)$, implying $s \geq (8r+3)/2$– in order to use all of $\mathcal{A}$. Thus, we consider specificaly the case $r = 1$, $s = 6$. In that case, the space $\mathcal{F}$ is generated by the orthonormal basis

$$\phi_{-k}(t) = \frac{\cos(kt + \pi/4)}{\sqrt{\pi}} \qquad k = 6, \ldots, 2 \tag{14}$$

$$\phi_k(t) = \frac{\sin(kt + \pi/4)}{\sqrt{\pi}} \qquad r = 2, 3 \ldots, 6 \tag{15}$$

According to Maple, the optimal approximation $\alpha_i(t)$ to $\phi_i(t)$ by $\mathcal{P}_{-1}^{1,2}[t]$ is

$$\alpha_i(t) = \sqrt{\frac{2}{\pi}} \frac{A_{ij} \cos(t) + B_{ij} \sin(t) + C_{ij}}{D_{ij}} \tag{16}$$

where $i \in \{-6, \cdots, 6\}$ and $j = \lfloor \frac{2t}{\pi} \rfloor$ is the quadrant index, and the coefficients A_{ij}, B_{ij}, C_{ij} are given by table 1.

i	j	A_{ij}	B_{ij}	C_{ij}	D_{ij}
-6	0	$-376+224\pi-30\pi^2$	$-184+200\pi-42\pi^2$	$-148+144\pi-35\pi^2$	$(32-20\pi+\pi^3)105$
-6	1	$-184+200\pi-42\pi^2$	$376-224\pi+30\pi^2$	$148-144\pi+35\pi^2$	$(32-20\pi+\pi^3)105$
-6	2	$376-224\pi+30\pi^2$	$184-200\pi+42\pi^2$	$-148+144\pi-35\pi^2$	$(32-20\pi+\pi^3)105$
-6	3	$184-200\pi+42\pi^2$	$-376+224\pi-30\pi^2$	$148-144\pi+35\pi^2$	$(32-20\pi+\pi^3)105$
-5	0	-1	1	0	$3\pi-6$
-5	1	$5\pi-24$	$24-5\pi$	$8-6\pi$	$-240+30\pi+15\pi^2$
-5	2	-1	1	0	$3\pi-6$
-5	3	$5\pi-24$	$24-5\pi$	$6\pi-8$	$-240+30\pi+15\pi^2$
-4	0	$128-12\pi-10\pi^2$	$-128+20\pi+6\pi^2$	$-16+8\pi$	$(32-20\pi+\pi^3)15$
-4	1	$128-20\pi-6\pi^2$	$128-20\pi-10\pi^2$	$-16+8\pi$	$(32-20\pi+\pi^3)15$
-4	2	$-128+12\pi+10\pi^2$	$128-20\pi-6\pi^2$	$8\pi-16$	$(32-20\pi+\pi^3)15$
-4	3	$-128+20\pi+6\pi^2$	$128+12\pi+10\pi^2$	$8\pi+16$	$(32-20\pi+\pi^3)15$
-3	0	$8-3\pi$	$8-3\pi$	$8-2\pi$	$-48+6\pi+3\pi^2$
-3	1	1	1	0	$\pi-2$
-3	2	$8-3\pi$	$8-3\pi$	$2\pi-8$	$-48+6\pi+3\pi^2$
-3	3	1	1	0	$\pi-2$
-2	0	$-56+24\pi-2\pi^2$	$8+16\pi-6\pi^2$	$-20+16\pi-3\pi^2$	$96-60\pi+3\pi^3$
-2	1	$8+16\pi-6\pi^2$	$56-24\pi+2\pi^2$	$20-16\pi+3\pi^2$	$96-60\pi+3\pi^3$
-2	2	$56-24\pi+2\pi^2$	$-8-16\pi+6\pi^2$	$-20+16\pi-3\pi^2$	$96-60\pi+3\pi^3$
-2	3	$-8-16\pi+6\pi^2$	$-56+24\pi-2\pi^2$	$20-16\pi+3\pi^2$	$96-60\pi+3\pi^3$
2	0	$-8-16\pi+6\pi^2$	$56-24\pi+2\pi^2$	$20-16\pi+3\pi^2$	$96-60\pi+3\pi^3$
2	1	$56-24\pi+2\pi^2$	$8+16\pi-6\pi^2$	$-20+16\pi-3\pi^2$	$96-60\pi+3\pi^3$
2	2	$8+16\pi-6\pi^2$	$-56+24\pi-2\pi^2$	$20-16\pi+3\pi^2$	$96-60\pi+3\pi^3$
2	3	$-56+24\pi-2\pi^2$	$-8-16\pi+6\pi^2$	$-20+16\pi-3\pi^2$	$96-60\pi+3\pi^3$
3	0	1	-1	0	$\pi-2$
3	1	$8-3\pi$	$3\pi-8$	$2\pi-8$	$-48+6\pi+3\pi^2$
3	2	1	-1	0	$\pi-2$
3	3	$8-3\pi$	$3\pi-8$	$8-2\pi$	$-48+6\pi+3\pi^2$
4	0	$-128+20\pi+6\pi^2$	$128-12\pi-10\pi^2$	$-16+8\pi$	$(32-20\pi+\pi^3)15$
4	1	$-128+12\pi+10\pi^2$	$-128+20\pi+6\pi^2$	$-16+8\pi$	$(32-20\pi+\pi^3)15$
4	2	$128-20\pi-6\pi^2$	$-128+6\pi+10\pi^2$	$-16+8\pi$	$(32-20\pi+\pi^3)15$
4	3	$128-12\pi-10\pi^2$	$128-20\pi-6\pi^2$	$-16+8\pi$	$(32-20\pi+\pi^3)15$
5	0	$5\pi-24$	$-24+5\pi$	$6\pi-8$	$-240+30\pi+15\pi^2$
5	1	-1	-1	0	$3\pi-6$
5	2	$5\pi-24$	$-24+5\pi$	$8-6\pi$	$-240+30\pi+15\pi^2$
5	3	-1	-1	0	$3\pi-6$
6	0	$184-200\pi+42\pi^2$	$376-224\pi+30\pi^2$	$148-144\pi+35\pi^2$	$(32-20\pi+\pi^3)105$
6	1	$376-224\pi+30\pi^2$	$-184+200\pi-42\pi^2$	$-148+144\pi-35\pi^2$	$(32-20\pi+\pi^3)105$
6	2	$-184+200\pi-42\pi^2$	$-376+224\pi-30\pi^2$	$148-144\pi+35\pi^2$	$(32-20\pi+\pi^3)105$
6	3	$-376+224\pi-30\pi^2$	$184-200\pi+42\pi^2$	$-148+144\pi-35\pi^2$	$(32-20\pi+\pi^3)105$

Table 1: Coefficients of $\alpha_i(t)$ in quadrant j, as per formula (16).

The basis functions ϕ_i, α_i, and ε_i are shown in figures 1–10 below.

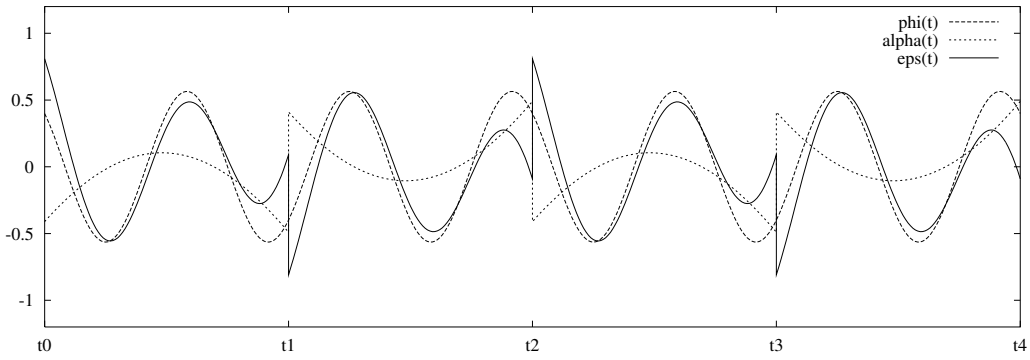

Figure 1: The basis functions $\phi_{-6}(t)$, $\alpha_{-6}(t)$, and $\varepsilon_{-6}(t)$.

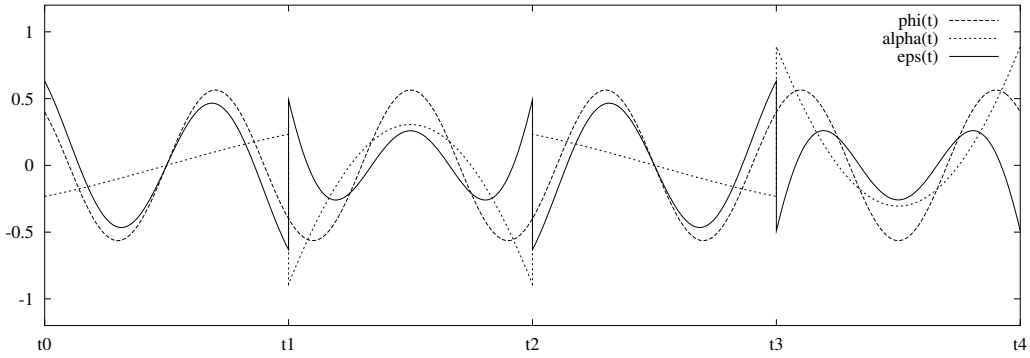

Figure 2: The basis functions $\phi_{-5}(t)$, $\alpha_{-5}(t)$, and $\varepsilon_{-5}(t)$.

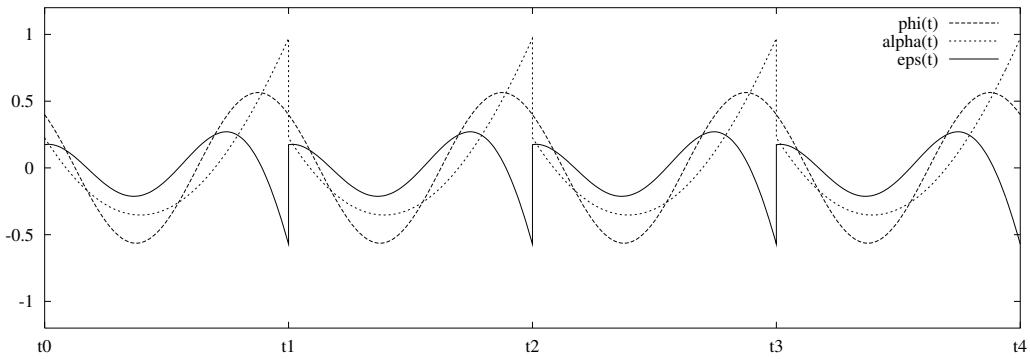

Figure 3: The basis functions $\phi_{-4}(t)$, $\alpha_{-4}(t)$, and $\varepsilon_{-4}(t)$.

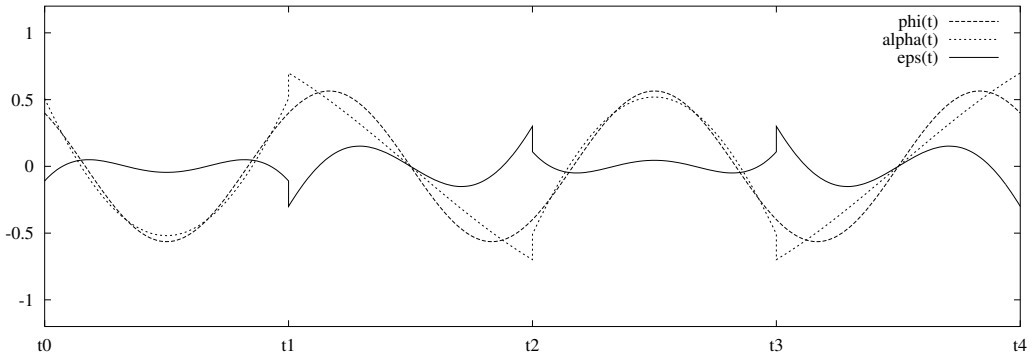

Figure 4: The basis functions $\phi_{-3}(t)$, $\alpha_{-3}(t)$, and $\varepsilon_{-3}(t)$.

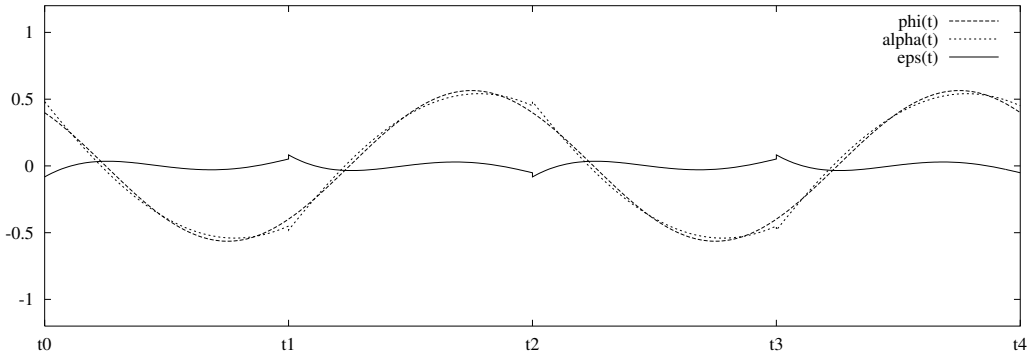

Figure 5: The basis functions $\phi_{-2}(t)$, $\alpha_{-2}(t)$, and $\varepsilon_{-2}(t)$.

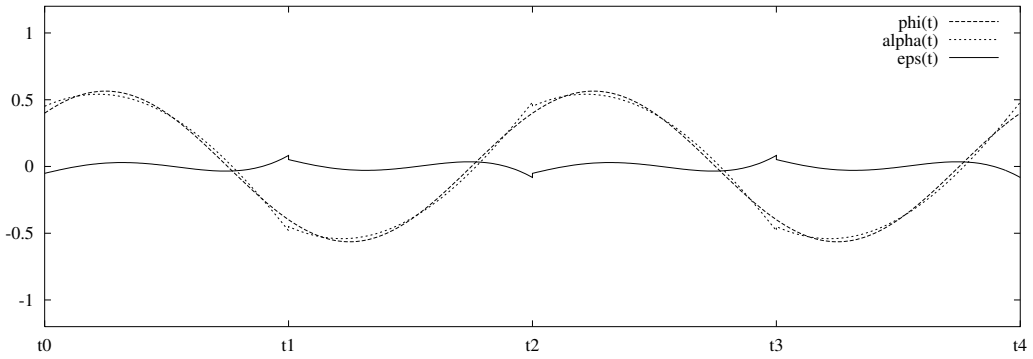

Figure 6: The basis functions $\phi_{+2}(t)$, $\alpha_{+2}(t)$, and $\varepsilon_{+2}(t)$.

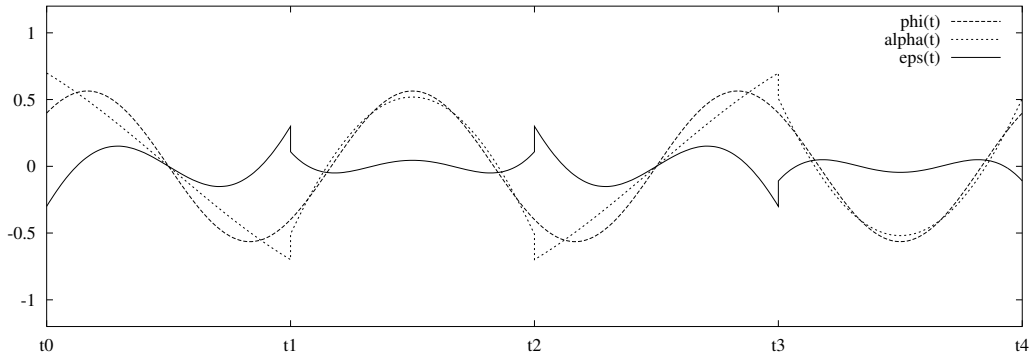

Figure 7: The basis functions $\phi_{+3}(t)$, $\alpha_{+3}(t)$, and $\varepsilon_{+3}(t)$.

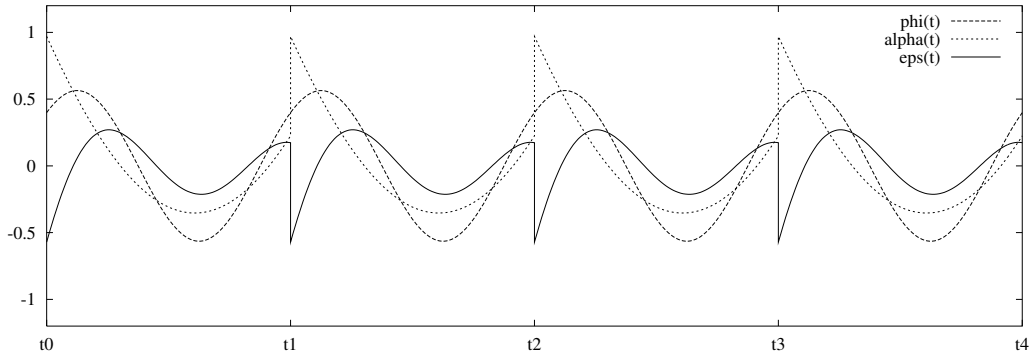

Figure 8: The basis functions $\phi_{+4}(t)$, $\alpha_{+4}(t)$, and $\varepsilon_{+4}(t)$.

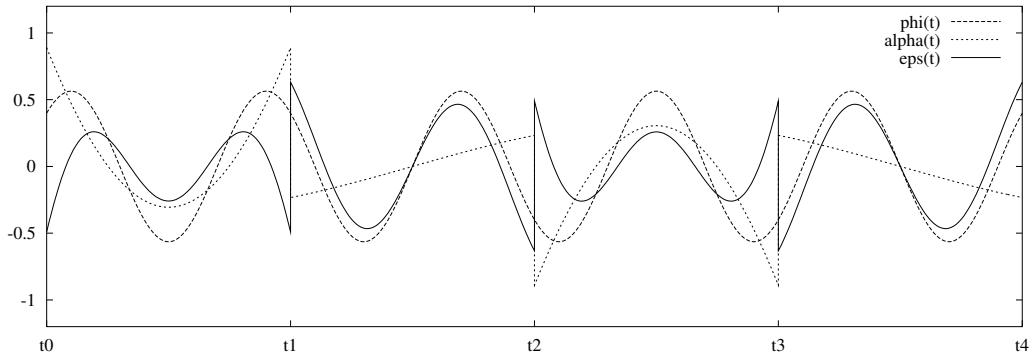

Figure 9: The basis functions $\phi_{+5}(t)$, $\alpha_{+5}(t)$, and $\varepsilon_{+5}(t)$.

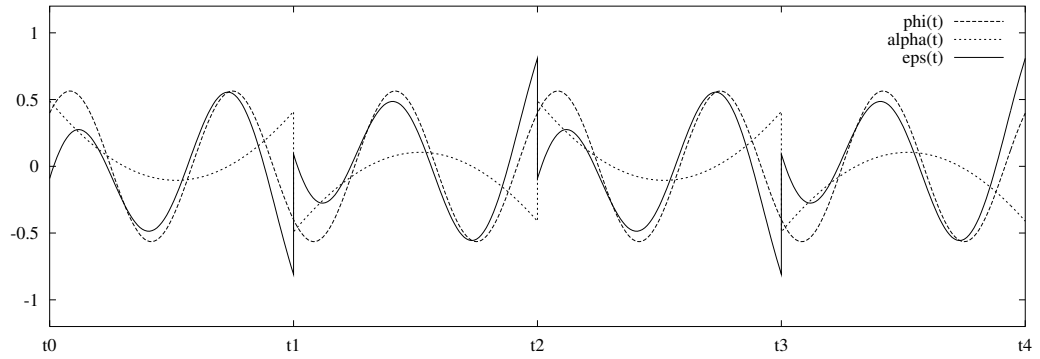

Figure 10: The basis functions $\phi_{+6}(t)$, $\alpha_{+6}(t)$, and $\varepsilon_{+6}(t)$.

Figure 11 shows the resulting error map $\mu_{\mathcal{A},\mathcal{F}}(x)$.

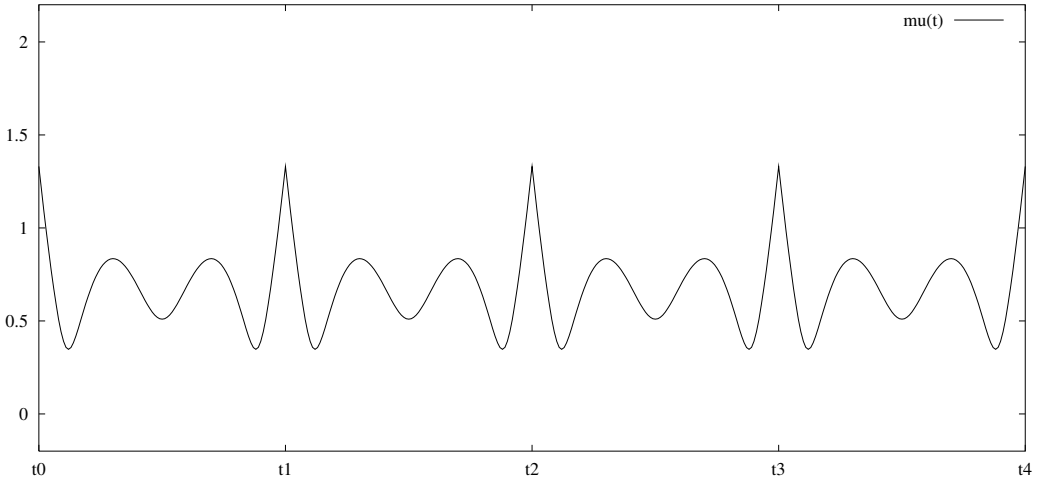

Figure 11: The error map $\mu_{\mathcal{A},\mathcal{F}}(t)$ for non-continuous trigonometric splines on four equal intervals, tested with the space of trigonometric polynomials of order 6.

5.2 Adaptive trigonometric splines on the circle

In the following example, the approximation space $\mathcal{A}$ consists of trigonometric splines of order $r = 2$ and continuity 0, defined on a subdivision T of the unit circle into $n = 8$ *unequal* intervals. Specifically, T consists of the intervals I_0 through I_7 shown below

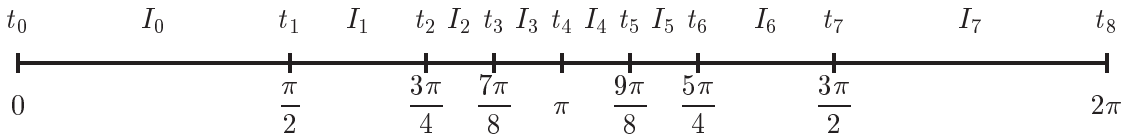

Within each interval I_j, the generic approximant is a linear combination g_j of the Fourier basis functions ϕ_i, for $-r \le i \le +r$. These partial functions are constrained to be continuous across interval boundaries; i.e. $g_{j-1}(t_j) = g_j(t_j)$ for each j in $\{0..n-1\}$ (where all indices are taken modulo n). These equations turn out to be independent, therefore the space $\mathcal{A}$ has dimension $n * (2r + 1) - n = 32$. For the gauge space $\mathcal{F}$, we will use the trigonometric polynomials of some order $s \ge r$, i.e. linear combinations of the basis functions ϕ_i for $-s \le i \le +s$. The order s must satisfy $2s + 1 \ge \dim \mathcal{A} = 32$, so we choose $s = 16$. Figures 12–17 show the basis functions ϕ_i, α_i, and ε_i for selected frequencies i.

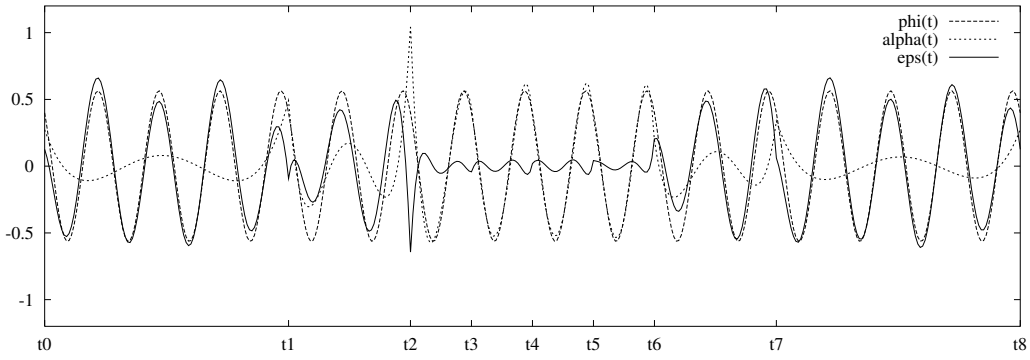

Figure 12: The basis functions $\phi_{-16}(t)$, $\alpha_{-16}(t)$, and $\varepsilon_{-16}(t)$.

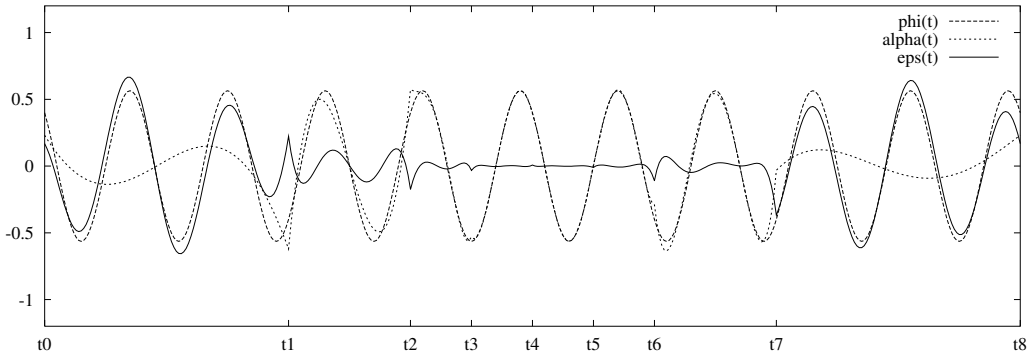

Figure 13: The basis functions $\phi_{-10}(t)$, $\alpha_{-10}(t)$, and $\varepsilon_{-10}(t)$.

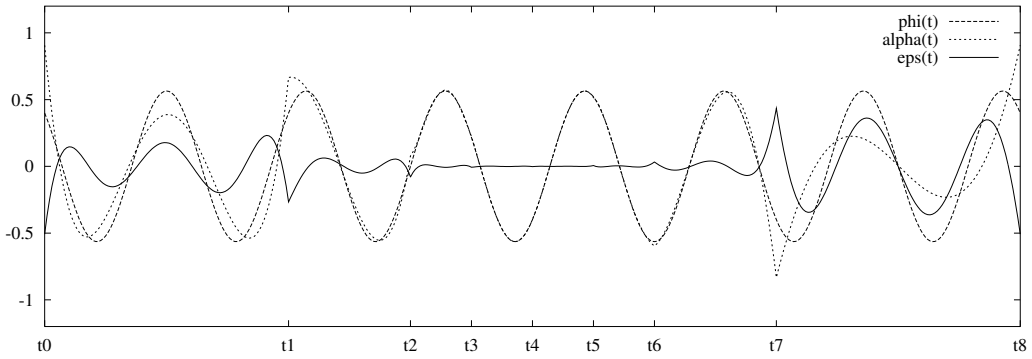

Figure 14: The basis functions $\phi_{-7}(t)$, $\alpha_{-7}(t)$, and $\varepsilon_{-7}(t)$.

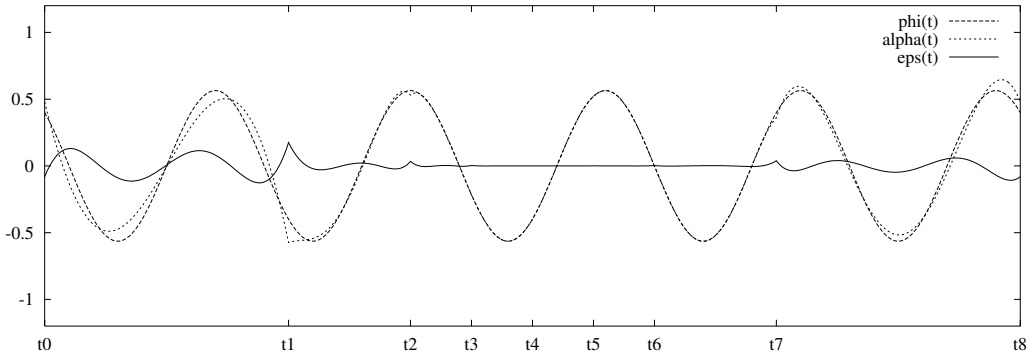

Figure 15: The basis functions $\phi_{-5}(t)$, $\alpha_{-5}(t)$, and $\varepsilon_{-5}(t)$.

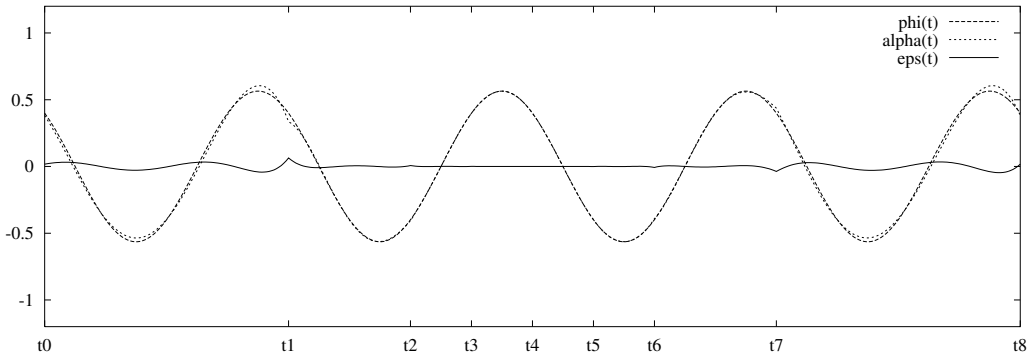

Figure 16: The basis functions $\phi_{-4}(t)$, $\alpha_{-4}(t)$, and $\varepsilon_{-4}(t)$.

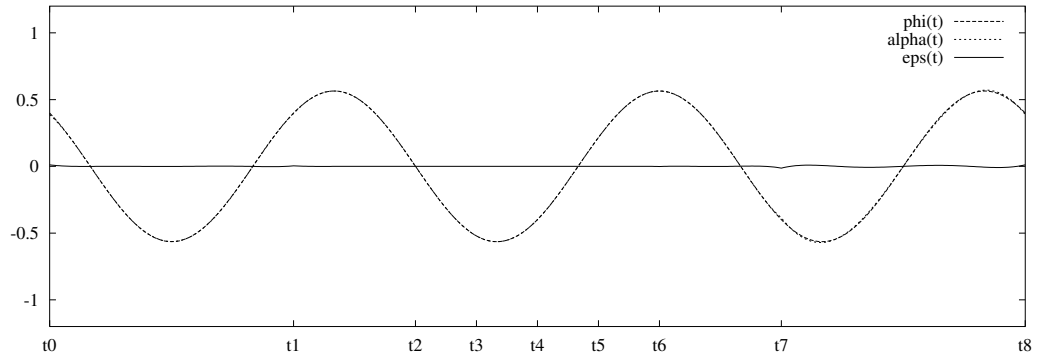

Figure 17: The basis functions $\phi_{-3}(t)$, $\alpha_{-3}(t)$, and $\varepsilon_{-3}(t)$.

Figure 18 shows the resulting error map $\mu_{\mathcal{A},\mathcal{F}}(x)$.

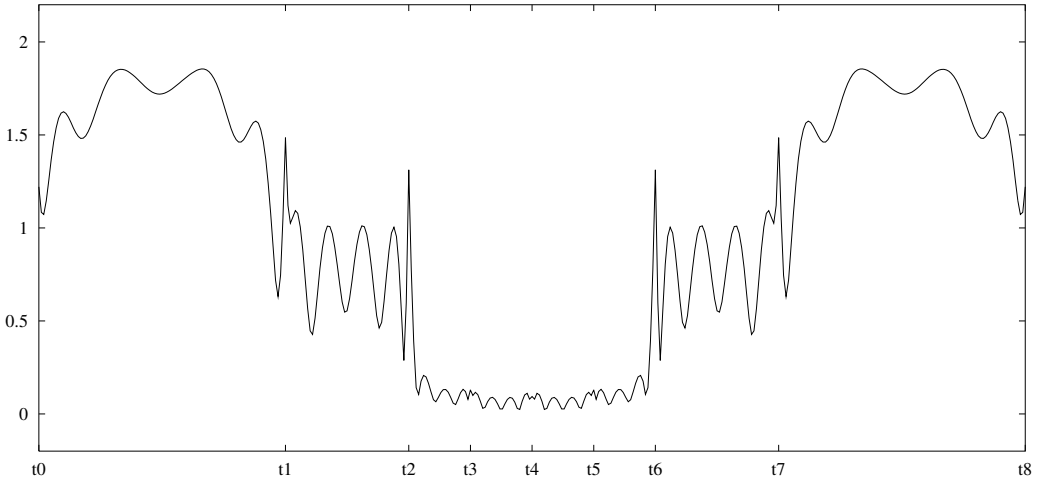

Figure 18: The error map $\mu_{\mathcal{A},\mathcal{F}}(t)$ for continuous (C_0) trigonometric splines on eight unequal intervals, tested with the space of trigonometric polynomials of order 16.

5.3 Homogeneous spherical splines of degree 2

In this and the following examples, the approximation spaces are spherical polynomial splines [4, 3, 2] of continuity class zero and various degrees, homogeneous and non-homogeneous, defined on the regular icosahedral triangulation T of the sphere $\mathbf{S}^2$.

Figure 19 shows the approximation error map $\mu_{\mathcal{A},\mathcal{F}}(p)$ for the homogeneous spherical spline space $\mathcal{A} = \mathcal{H}_0^2[T]/\mathbf{S}^2$, which has dimension 42. This is the lowest-degree homogeneous space wich has an Alfeld-Neamtu-Schumeker basis [1] The gauge space $\mathcal{F}$ is the family $\mathcal{Y}_6^2$ of spherical harmonics of maximum order 6, which has dimension 49. (The intersection of the two spaces is the family of spherical harmonics of even order ≤ 2, of dimension 6; therefore, the relevant subspaces $\mathcal{A}'$ and $\mathcal{F}'$ have dimensions 36 and 43, respectively.)

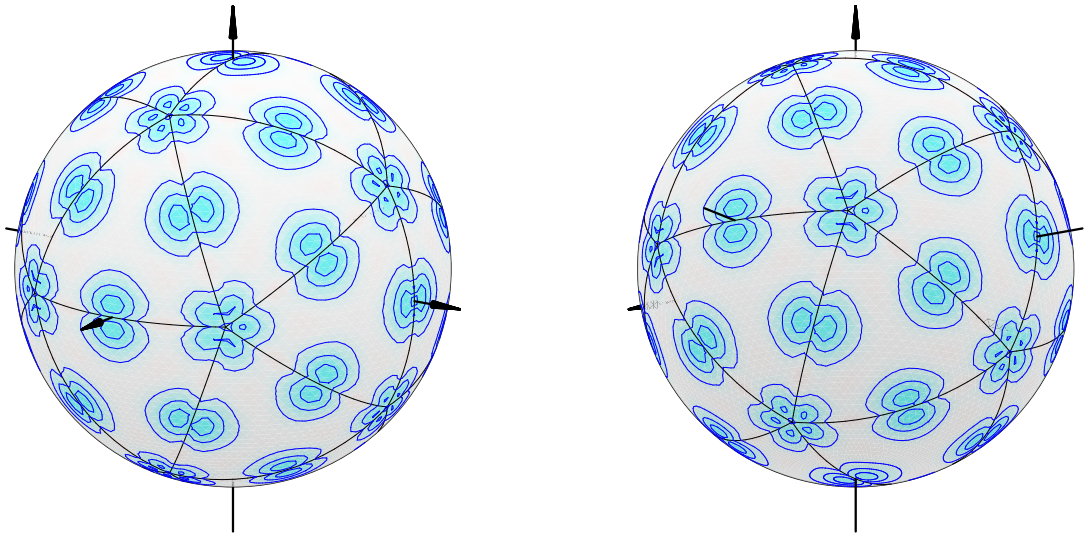

front rear

Figure 19: Error map for the approximation space $\mathcal{A} = \mathcal{H}_0^2[T]/\mathbf{S}^2$, tested with the gauge space $\mathcal{F} = \mathcal{Y}_6^2$. The maximum value of the error map is 1.25. The level curves are logarithmically spaced (5 per decade).

5.4 Non-homogeneous spherical splines of degree 3

Figure 20 shows the approximation error map for the homogeneous spherical spline space $\mathcal{A} = \mathcal{P}_0^3[T]/\mathbf{S}^2$, which has dimension 134. This is the lowest degree non-homogeneous space whose basis can be obtained by joining two Alfeld-Neamtu-Schumeker bases [1] The gauge space $\mathcal{F}$ is the family $\mathcal{Y}_{11}^2$ of spherical harmonics of maximum order 11, which has dimension 144. (Their intersection is $\mathcal{Y}_3^2$ which as has dimension 16, so the relevant subspaces $\mathcal{A}'$ and $\mathcal{F}'$ have dimensions 118 and 128, respectively.)

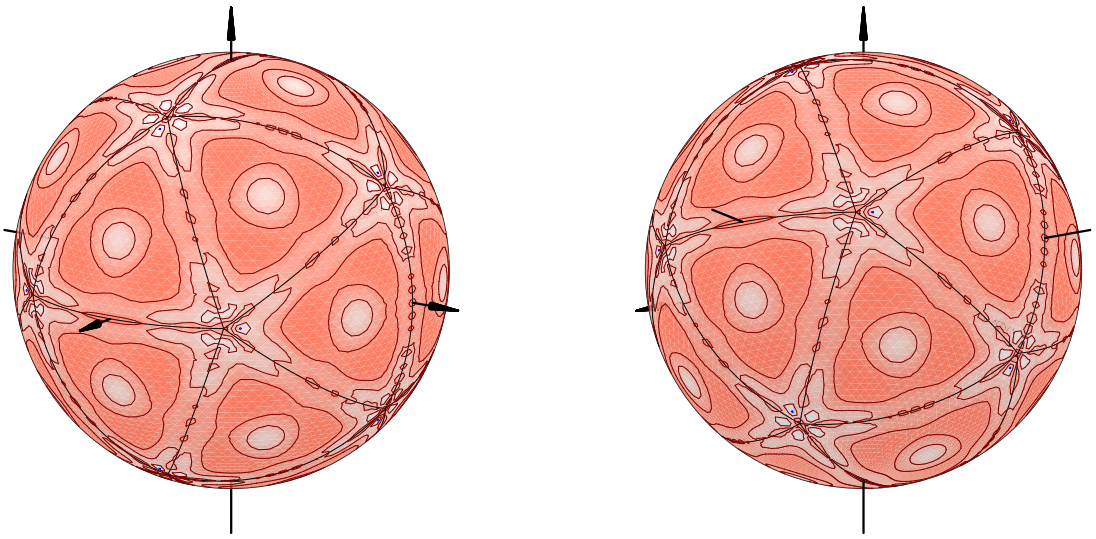

front rear

Figure 20: Error map for the approximation space $\mathcal{A} = \mathcal{P}_0^3[T]/\mathbf{S}^2$, tested with the gauge space $\mathcal{F} = \mathcal{Y}_{11}^2$. The maximum value of the error map is 4.38. The level curves are logarithmically spaced (5 per decade).

5.5 Homogeneous spherical splines of degree 5

Figure 21 shows the approximation error map $\mu_{\mathcal{A},\mathcal{F}}(p)$ for the homogeneous spherical spline space $\mathcal{A} = \mathcal{H}^5_0[T]/\mathbf{S}^2$, which has dimension 252. This is the lowest-degree homogeneous space wich has an Alfeld-Neamtu-Schumeker basis [1]. The gauge space $\mathcal{F}$ is the family $\mathcal{Y}^2_{15}$ of spherical harmonics of maximum order 15, which has dimension 256. (The intersection of the two spaces is the family of spherical harmonics of odd order ≤ 5, which has dimension 21; therefore, the relevant subspaces $\mathcal{A}'$ and $\mathcal{F}'$ have dimensions 231 and 235, respectively.)

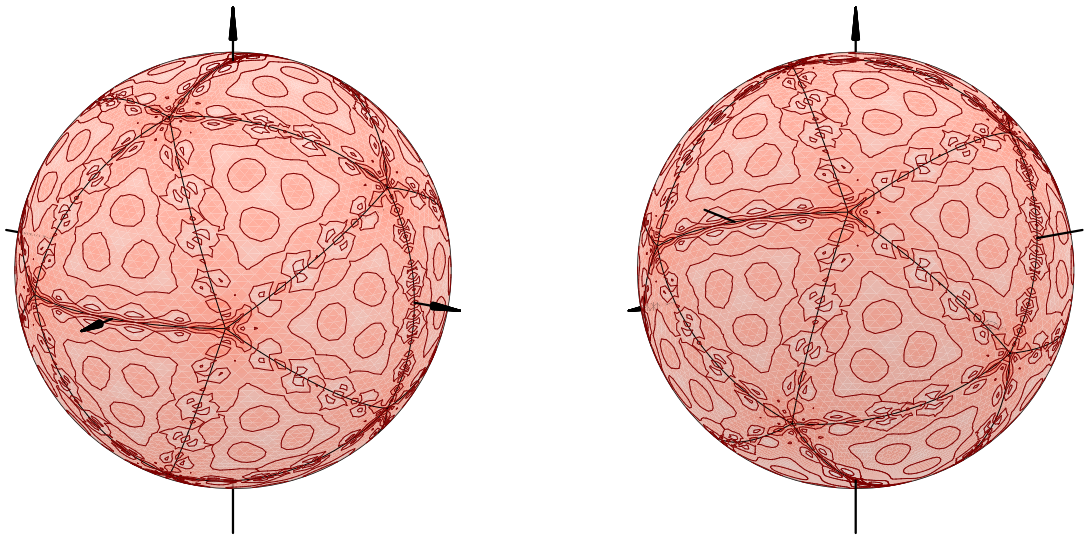

front rear

Figure 21: Error map for the approximation space $\mathcal{A} = \mathcal{H}^5_0[T]/\mathbf{S}^2$, tested with the gauge space $\mathcal{F} = \mathcal{Y}^2_{15}$. The maximum value of the error map is 1.35×10^1. The level curves are logarithmically spaced (5 per decade).

5.6 Non-homogeneous spherical splines of degree 4

Figure 22 shows the approximation error map $\mu_{\mathcal{A},\mathcal{F}}(p)$ for the homogeneous spherical spline space $\mathcal{A} = \mathcal{P}_0^4[T]/\mathbf{S}^2$, which has dimension 254. The gauge space $\mathcal{F}$ is the family $\mathcal{Y}_{15}^2$ of spherical harmonics of maximum order 15, which has dimension 256. (Their intersection is $\mathcal{Y}_4^2$ which as has dimension 25, so the relevant subspaces $\mathcal{A}'$ and $\mathcal{F}'$ have dimensions 229 and 231, respectively.)

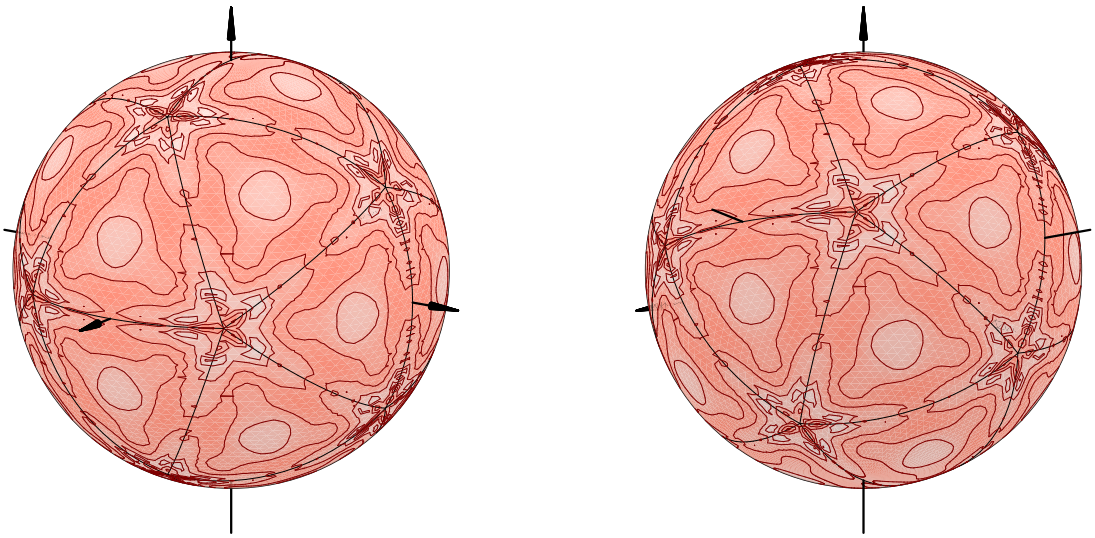

front rear

Figure 22: Error map for the approximation space $\mathcal{A} = \mathcal{P}_0^4[T]/\mathbf{S}^2$, tested with the gauge space $\mathcal{F} = \mathcal{Y}_{15}^2$. The maximum value of the error map is 9.37. The level curves are logarithmically spaced (5 per decade).

5.7 Homogeneous spherical splines of degree 2 on a variable mesh

For the next four examples, the triangulation T' has icosahedral topology, but its geometry was skewed so as to provide regions of very different sizes.

Figure 23 shows the approximation error map $\mu_{\mathcal{A},\mathcal{F}}(p)$ for the homogeneous spherical spline space $\mathcal{A} = \mathcal{H}_0^2[T']/\mathbf{S}^2$, which has dimension 42. The gauge space $\mathcal{F}$ is the family $\mathcal{Y}_6^2$ of spherical harmonics of maximum order 6, which has dimension 49. (The intersection of the two spaces is the family of spherical harmonics of even order ≤ 2, of dimension 6; therefore, the relevant subspaces $\mathcal{A}'$ and $\mathcal{F}'$ have dimensions 36 and 43, respectively.)

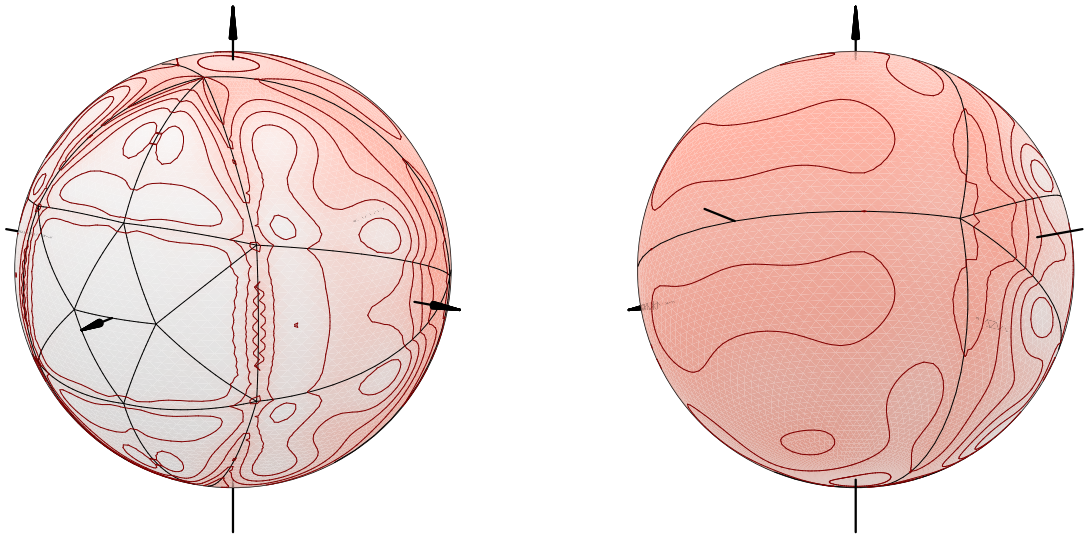

front rear

Figure 23: Error map for the approximation space $\mathcal{A} = \mathcal{H}_0^2[T]/\mathbf{S}^2$, tested with the gauge space $\mathcal{F} = \mathcal{Y}_6^2$. The maximum value of the error map is 3.13. The level curves are logarithmically spaced (5 per decade).

5.8 Non-homogeneous spherical splines of degree 3 on a variable mesh

Figure 24 shows the approximation error map $\mu_{\mathcal{A},\mathcal{F}}(p)$ for the homogeneous spherical spline space $\mathcal{A} = \mathcal{P}_0^3[T']/\mathbf{S}^2$, which has dimension 134. The gauge space $\mathcal{F}$ is the family $\mathcal{Y}_{11}^2$ of spherical harmonics of maximum order 11, which has dimension 144. (Their intersection is $\mathcal{Y}_3^2$ which as has dimension 16, so the relevant subspaces $\mathcal{A}'$ and $\mathcal{F}'$ have dimensions 118 and 128, respectively.)

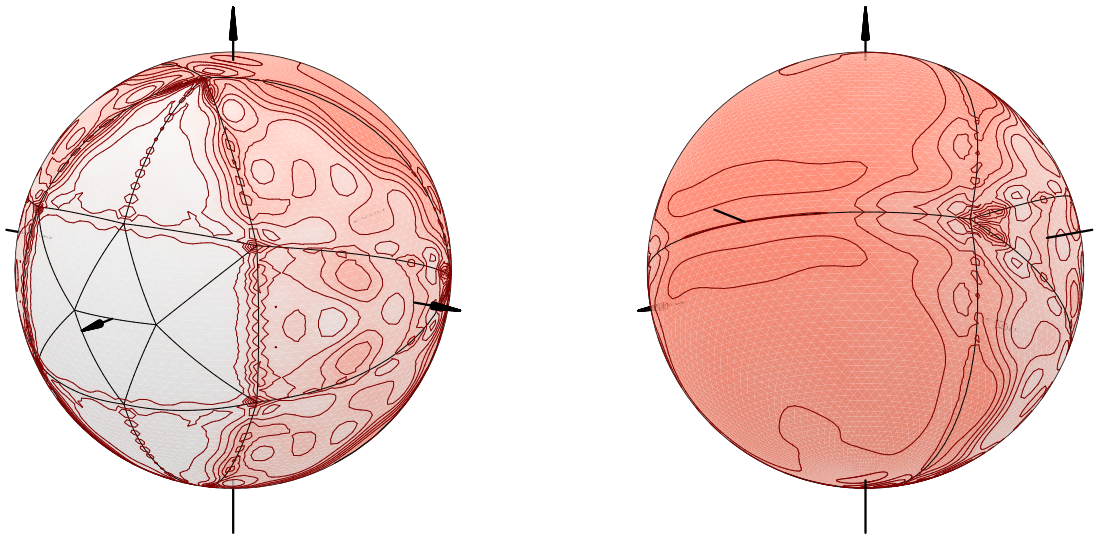

front rear

Figure 24: Error map for the approximation space $\mathcal{A} = \mathcal{P}_0^3[T]/\mathbf{S}^2$, tested with the gauge space $\mathcal{F} = \mathcal{Y}_{11}^2$. The maximum value of the error map is 8.8. The level curves are logarithmically spaced (5 per decade).

5.9 Homogeneous spherical splines of degree 5 on a variable mesh

Figure 25 shows the approximation error map $\mu_{\mathcal{A},\mathcal{F}}(p)$ for the homogeneous spherical spline space $\mathcal{A} = \mathcal{H}_0^5[T']/\mathbf{S}^2$, which has dimension 252. The gauge space $\mathcal{F}$ is the family $\mathcal{Y}_{15}^2$ of spherical harmonics of maximum order 15, which has dimension 256. (The intersection of the two spaces is the family of spherical harmonics of odd order ≤ 5, which has , dimension 21; therefore, the relevant subspaces $\mathcal{A}'$ and $\mathcal{F}'$ have dimensions 231 and 235, respectively.)

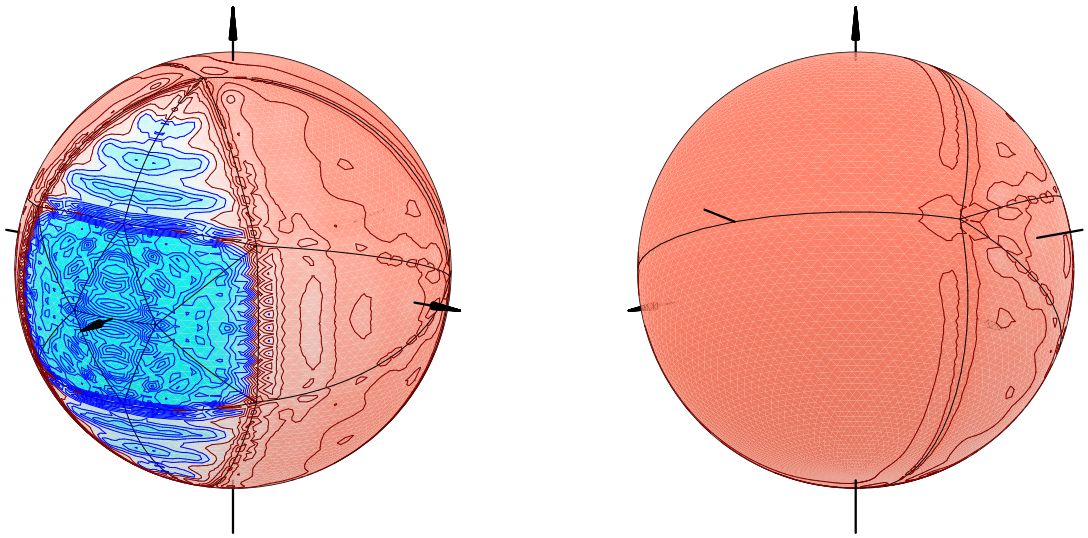

front rear

Figure 25: Error map for the approximation space $\mathcal{A} = \mathcal{H}_0^5[T]/\mathbf{S}^2$, tested with the gauge space $\mathcal{F} = \mathcal{Y}_{15}^2$. The maximum value of the error map is 1.71×10^1. The level curves are logarithmically spaced (5 per decade).

5.10 Non-homogeneous spherical splines of degree 4 on a variable mesh

Figure 26 shows the approximation error map $\mu_{\mathcal{A},\mathcal{F}}(p)$ for the homogeneous spherical spline space $\mathcal{A} = \mathcal{P}_0^4[T']/\mathbf{S}^2$, which has dimension 254. The gauge space $\mathcal{F}$ is the family $\mathcal{Y}_{15}^2$ of spherical harmonics of maximum order 15, which has dimension 256. (Their intersection is $\mathcal{Y}_4^2$ which as has dimension 25, so the relevant subspaces $\mathcal{A}'$ and $\mathcal{F}'$ have dimensions 229 and 231, respectively.)

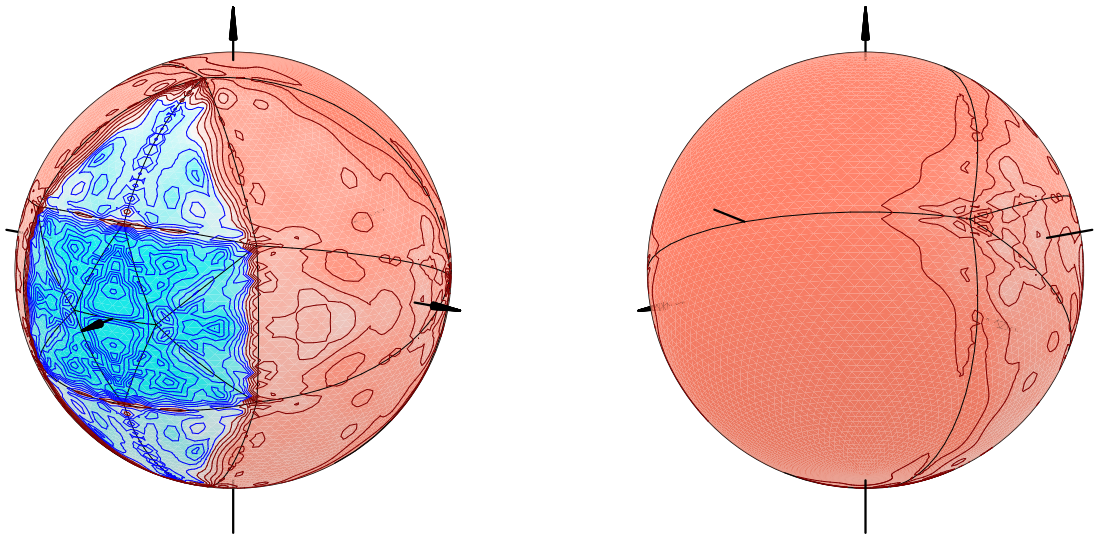

front rear

Figure 26: Error map for the approximation space $\mathcal{A} = \mathcal{P}_0^4[T]/\mathbf{S}^2$, tested with the gauge space $\mathcal{F} = \mathcal{Y}_{15}^2$. The maximum value of the error map is 1.79×10^1. The level curves are logarithmically spaced (5 per decade).

References

[1] Peter Alfeld, Marian Neamtu, and Larry L. Schumaker. Dimension and local bases of homogeneous spline spaces. *SIAM Journal of Mathematical Analysis*, 27(5):1482–1501, September 1996.

[2] Anamaria Gomide. *Splines Polinomiais Não Homogêneos na Esfera*. PhD thesis, Institute of Computing, University of Campinas, May 1999.

[3] Anamaria Gomide and Jorge Stolfi. Bases for non-homogeneous polynomial $\mathbf{C}_k$ splines on the sphere. In *Lecture Notes in Computer Science 1380: Proc. LATIN'98 - Latin American Theoretical Informatics Conference*, pages 133–140. Springer, April 1998.

[4] Anamaria Gomide and Jorge Stolfi. Non-homogeneous polynomial C_k splines on the sphere S^n. Technical Report IC-00-10, Institute of Computing, Univ. of Campinas, July 2000.

[5] I. S. Gradshtein and I. M. Ryzhik. *Table of Integrals, Series, and Products*. Academic Press, fifth edition, 1994.

[6] Mike Neamtu and Larry L. Schumaker. Approximation properties of splines on spherical triangulations. In *Abstracts of the 4th International AFA Conference on Curves and Surfaces*, page 59, Saint-Malo, France, June 1999.